Low-Dose Dual-Source Computed Tomography for Evaluating Persistent Truncus Arteriosus Associated with Cardiovascular Anomalies: Comparison with Transthoracic Echocardiography

Si-shi Tang
Sichuan University
Qi-ling Wang
Peking University Shenzhen Hospital
Ke Shi
Sichuan University
Ying-kun Guo
Sichuan University
Li Jiang
Sichuan University
Jin Wang
Sichuan University
Yuan Li
Sichuan University
Zhi-gang Yang (yangzg666@163.com)
Sichuan University

Research Article

Keywords: Low-dose, dual-source computed tomography, persistent truncus arteriosus, cardiovascular anomalies, transthoracic echocardiography

Posted Date: June 9th, 2021

DOI: https://doi.org/10.21203/rs.3.rs-583538/v1

Abstract

Background

To assess the morphological features of persistent truncus arteriosus (PTA) on low-dose dual-source computed tomography (DSCT) and compare its diagnostic value for associated cardiovascular anomalies with that of transthoracic echocardiography (TTE).

Methods:

Twenty-four PTA patients were enrolled in this retrospective study. The types of PTA, diameters of the truncus artery (TA), main pulmonary artery (MPA), right pulmonary artery (RPA), left pulmonary artery (LPA), and ventricular septal defect (VSD) on DSCT were recorded. Besides, all associated cardiovascular abnormalities were assessed. The diagnostic performance of DSCT and TTE for associated anomalies were compared. The effective doses of DSCT were calculated.

Results:

Four types were found: type A1(n=13/24, 54.17%), type A2(n=7/24, 29.16%), type A3（n=3/24, 12.50%）and type A4(n=1/24,4.17%). The mean diameter of VSD, TA, MPA, RPA, and LPA was 1.47±0.56cm, 3.92±1.56cm, 2.27±1.65cm, 1.48±0.74cm and 1.38±0.66cm, respectively. 78 associated cardiovascular anomalies were confirmed. The most common associated abnormalities were VSD (100%), right-sided aortic arch (33.33%) and aortopulmonary collateral vessels (29.17%). Although TTE was better at diagnosing intracardiac anomalies (accuracy:99.17% vs. 95%; sensitivity: 97.06% vs. 88.24%; specificity: 100% vs. 97.67%), DSCT had an advantage in diagnosing the associated cardiovascular abnormalities (accuracy: 98.61% vs. 96.07%; sensitivity: 94.87% vs. 82.05%; specificity: 99.44% vs. 99.15%). The estimated mean effective doses was 0.98±0.37mSv (1mSv).

Conclusions:

Low-dose DSCT could accurately confirm the morphological features of PTA. Compared to TTE, low-dose DSCT is a better diagnostic tool for associated cardiovascular abnormalities. Combining with TTE will be beneficial to provide more accurate information for clinical interventions.

1. Introduction

Persistent truncus arteriosus (PTA) is a rare congenital cardiac malformation, accounting for 0.7–1.4 % of all congenital heart abnormalities [1]. It is characterized by a single arterial trunk originating from the heart's ventricles and supplying systemic, coronary, and pulmonary circulations（2）. Early surgical intervention is the primary treatment for PTA patients. About 90% of PTA patients would die in the first year of life without surgery, many during the early infancy（3）. The optimal timing and strategies for surgical repair are based on the morphological features. Thus, the accurate preoperative diagnosis and description of anatomy are crucial. Moreover, the associated anomalies, especially the coronary and pulmonary artery abnormalities, aortopulmonary collateral arteries, are associated with the surgical process and mortality [4–6].

Transthoracic echocardiography(TTE)is the first imaging modality for congenital heart disease. However, its disadvantages, such as operator-dependent essence, small acoustic window, make it inadequate to exhibit the extracardiac structures [7]. Low-dose dual-source computed tomography (DSCT), with low radiation dose, excellent image quality, and powerful post-processing techniques, can evaluate intracardiac and extracardiac malformations. It has been widely applied to cardiovascular examinations in recent years [8–13]. To the best of our knowledge, original researches with a certain number of patients focusing on the preoperative evaluation on DSCT were rare [14–16]. Therefore, the purpose of this study is to comprehensively assess the morphological features of PTA on low-dose DSCT and compare its diagnostic accuracy for associated cardiovascular anomalies with that of TTE.

2. Materials And Methods

2.1. Study population

From January 2010 to September 2020, a total of 32 patients with PTA in our hospital were retrospectively enrolled. They were confirmed by surgery or conventional cardiac angiography (CCA). The exclusion criteria included:(a) unavailable data for the DSCT or

TTE (n = 5), (b) incomplete clinical data (n = 3). Finally,24 patients remained, including 12 females and 12males (mean age: 9.78 ± 10.12 years, ranging from 1 month to 32 years).

This study was performed in line with the principles of the Declaration of Helsinki. Approval was granted by Biomedical Research Ethics Committee of our hospital, Sichuan University (Chengdu, Sichuan, China; No.14–163), and informed consent was waived off. The sensitive information of the participants was protected with complete confidentiality and only used for this research.

2.2. Dual-source computed tomography

All scans were performed with a DSCT scanner (Somatom Definition; Siemens Medical Solutions, Forchheim, Germany). Patients younger than six years were administered short-term sedative (chloral hydrate at a concentration of 10%, 0.5 ml/kg) before the examination. Older patients were trained to hold their breath during scanning with full cooperation. The scans were performed from the thorax inlet to 2 cm below the diaphragm in the craniocaudal direction. All patients received the nonionic contrast agent (iopamidol, 370 mg/ml, Bracco, Italy) via an antecubital vein, at a rate of 1.2–2.5ml/s, followed by 20 ml of saline solution at the same flow velocity. The total injected volume was determined by body weight (1.5 ml/kg). A retrospective electrocardiography (ECG)-gated protocol was applied. The acquisition parameters were as follows: tube voltage, 80–120 kV; tube current, automatic adjustment; gantry rotation time, 0.28 s and pitch, 0.2–0.5 (adapted to heart rate; higher heart rate used a higher pitch). The ECG-pulsing window was set to auto. Bolus tracking technique was applied in the region of interest (ROI) in the descending aorta, with a predefined threshold of 100 HU. When the ROI attenuation threshold reached 100 HU, image acquisition was triggered following a delay of 5 seconds. All acquired data were processed on an external workstation (Syngo; Siemens Medical System, Forchheim, Germany). Images were reconstructed with a slice thickness of 0.75 mm and an increment of 0.7 mm. The multiplanar reformation, maximum intensity projection, and volume rendering were used to interpret the images.

2.3. Image analysis

The PTA classification system suggested by Van Praagh and Van Praagh was used as our standard of classification [17]. Type A and B represent the presence and absence of ventricular septal defect, respectively. Type A was classified into four types, namely A1, A2, A3, A4. CT images were analyzed blindly by two experienced cardiac radiologists with more than five years' experience. Types of PTA, origins of the truncus artery (TA), associated intracardiac and extracardiac malformations, the diameter of TA, main pulmonary artery (MPA), right pulmonary artery (RPA), left pulmonary artery (LPA), and ventricular septal defect (VSD) was measured. When the two radiologists disagreed on the findings, they discussed and reached a consensus. One radiologist's DSCT measurement was reanalyzed by the same radiologist two weeks later to determine the intra-observer variability. To determine the inter-observer variability, the other radiologist repeated the measurement blindly.

The associated cardiovascular malformations contained the intracardiac and extracardiac structures. To compare the diagnostic accuracy of DSCT with TTE, we categorized the confirmed malformations into six groups, namely intracardiac anomalies, anomalies of the aortic arch and its branches, the pulmonary vessels, aortopulmonary vessels, the systemic veins, and coronary artery anomalies.

2.4. Assessment of image quality

The overall image quality of DSCT was analyzed by the two radiologists mentioned above, using a four-point scale system. 4 represents excellent (excellent image quality, an incredible display of anatomic details). 3 illustrates good (good image quality, clear display of anatomic details). 2 represents fair (fair image quality, insufficient for a complete evaluation of anatomic details).1 illustrates poor (poor image quality, severe artifacts that make anatomic details incomplete or useless). A score of 3 or 4 was thought to be diagnostic.

2.5. Radiation dose estimation

Two radiation dose parameters, volume CT dose index (CTDIvol) and dose-length product (DLP), were automatically recorded during the examinations. The effective dose (ED) was derived from the DLP multiplied by age-specific DLP conversion coefficients, based on the 2007 recommendation of the International Commission on Radiological Protection [18]. These conversion coefficients were as follows:0.039 for patients aged younger than 4months,0.026 for patients aged between 4 months and 1 year, 0.018 for patients aged between 1 and 6 years, 0.012 for patients aged between 6 and 10 years, and 0.014 for those aged older than 10 years.

2.6. Trans-thoracic echocardiography

Standard TTE examinations were performed in all subjects using a Philips Sonos 7500 ultrasound system (Philips Medical Systems, Bothell, WA) based on the American Society of Echocardiography Committee [19]. A skilled echocardiographer with more than five years' experience blindly interpreted the TTE images.

2.7. Statistical analysis

The data were analyzed using SPSS software for Windows (version 24.0; IBM Corp., Armonk, NY, USA). Categorical variables were expressed as numbers and percentages. Continuous variables were presented as means ± standard deviations. The diagnostic performance of DSCT and TTE in associated cardiovascular malformations was expressed as accuracy, sensitivity, specificity, positive predictive value, and negative predictive value. Agreement of image quality was evaluated using the kappa value. Kappa values from 0.61 to 0.80, from 0.81 to 1.00 were considered as good and excellent agreement. The intraclass correlation coefficients (ICC) were calculated to evaluate the inter-observer and intra-observer variability.

3. Results

3.1. Baseline characteristics

The baseline characteristics of the patients were presented in Table 1. The most common clinical signs and symptoms were heart murmurs, post-exercising tachypnea, cyanosis, and easy cold.

Table 1
Baseline characteristics of patients with persistent truncus arteriosus

Variables	Total (n = 24)
Age, years	9.78 ± 10.12
Female, n (%)	12 (50%)
Body mass index (kg/m2)	15.71 ± 1.27
Heart rate (bpm)	104.41 ± 20.20
Systolic blood pressure (mmHg)	99.08 ± 16.28
Diastolic blood pressure (mmHg)	57.88 ± 13.38
Symptoms, n (%)	
Heart murmurs	23 (95.83%)
Post-exercising tachypnea	17(70.83%)
Cyanosis	11 (45.83%)
Easy Cold	8 (33.33%)
Developmental delay	6 (25.00%)
Feeding intolerance	3 (12.50%)
Aquatting phenomenon	2(8.33%)
Precordial region pain	1(4.17%)
Note: Data are presented as number of patients (percentage) or mean ± standard deviations.	

3.2. Morphological features and measurement on DSCT

Type A1 to A4 were found in our patients, and type B patient was not detected. The most and least common type was type A1 and A4, respectively (Figs. 1–4). These results were entirely consistent with the results confirmed by surgery or CCA. The average diameter of VSD、TA、MPA、RPA and LPA measured on DSCT was summarized in Table 2.

Table 2
Morphological features on dual-source computed tomography

Variables	Total (n = 24)
Types, n (%)	
Type A1	13(54.17%)
Type A2	7(29.16%)
Type A3	3(12.50%)
Type A4	1(4.17%)
Origin of TA, n (%)	
both ventricles	24(100%)
The average diameter of various parameters	
ventricular septal defect (cm)	1.46 ± 0.56
truncus artery (cm)	3.94 ± 1.45
main pulmonary artery(cm)	2.32 ± 1.67
right pulmonary artery(cm)	1.48 ± 0.66
left pulmonary artery(cm)	1.39 ± 0.58
Note: Data are presented as number of patients (percentage) or as mean ± standard deviations.	

3.3. Associated cardiovascular abnormalities

A total of 78 associated cardiovascular abnormalities were found in our patients. Among them, ventricular septal defect (100%), right-sided aortic arch (33.33%), and aortopulmonary collateral vessels (29.17%) are the most common concomitant anomalies (Figs. 1–5). The summary of findings obtained by DSCT and TTE was presented in Table 3.

Table 3 A summary of the associated cardiovascular abnormalities on DSCT and TTE (n = 24)

Associated cardiovascular anomalies	Surgical/ CCA Results	CT findings				TTE findings			
		TP	FN	TN	FP	TP	FN	TN	FP
Intracardiac anomalies									
Atrial septal defect	5(20.83%)	4	1	18	1	5	0	19	0
Ventricular septal defect	24(100%)	24	0	0	0	24	0	0	0
Three rooms in the left atrium	1(4.17%)	1	0	23	0	1	0	23	0
Bicuspid truncal valve	2(8.33%)	1	1	22	0	2	0	22	0
Quadricuspid truncal valve	2(8.33%)	0	2	21	1	1	1	22	0
Extracardiac vascular anomalies									
Anomalies of aortic and its branches									
Interrupted aortic arch	1(4.17%)	1	0	23	0	1	0	23	0
Stenosis of aorta arch	1(4.17%)	1	0	23	0	1	0	23	0
Right-sided aortic arch	8(33.33%)	8	0	16	0	7	1	15	1
Aberrant subclavicular artery	6(25.00%)	6	0	18	0	5	1	18	0
Aortic arch's branches' origin anomalies	5(20.83%)	5	0	19	0	4	1	19	0
Anomalies of the pulmonary vessels									
Crossed Pulmonary artery	4(16.67%)	4	0	20	0	2	2	19	1
Pulmonary artery stenosis	3(12.50%)	3	0	21	0	1	2	21	0
Anomalous pulmonary venous drainage	1(4.17%)	1	0	23	0	1	0	23	0
Anomalies of the aortopulmonary vessels									
Aortopulmonary collateral vessels	7(29.17%)	7	0	17	0	5	2	16	1
Patent ductus arteriosus	1(4.17%)	1	0	23	0	1	0	23	0
Anomalies of the systemic veins									
Persistent left superior vena cava	3(12.50%)	3	0	21	0	2	1	21	0
Aberrant brachiocephalic vein	1(4.17%)	1	0	23	0	0	1	23	0
Coronary artery origin anomalies	3(12.50%)	3	0	21	0	1	2	21	0
Total	78	74	4	352	2	64	14	351	3

Abbreviations: DSCT, dual-source computed tomography; TTE, transthoracic echocardiography; CCA, conventional cardiac angiography; TP true positive finding; FN false negative finding; TN true negative finding; FP false positive finding

3.4 Comparison of diagnostic accuracy between DSCT and TTE

DSCT was superior to TTE in detecting associated cardiac vascular anomalies (accuracy: 98.61% vs. 96.07%; sensitivity: 94.87% vs. 82.05%; specificity: 99.44% vs. 99.15%; ppv: 97.37% vs. 95.52%; npv: 98.88% vs. 96.16%). Although TTE was better at diagnosing intracardiac anomalies (accuracy: 99.17% vs. 95%; sensitivity: 97.06% vs. 88.24%; specificity: 100% vs. 97.67%; ppv: 100% vs. 93.75%; npv: 98.85% vs. 95.46%), DSCT had advantages in diagnosing all the five groups of extra-cardiovascular anomalies (accuracy: 100% vs. 94.87%; sensitivity: 100% vs.70.46%; specificity: 100% vs. 98.88%; ppv:100% vs. 91.18%; npv: 100% vs. 95.32%). The accuracy, sensitivity, specificity, positive predictive value, and negative predictive value. of DSCT and TTE for each group were showed in Table 4.

Table 4
The diagnostic accuracy of DSCT and TTE according to anomalies categories.

Anomalies categories	DSCT					TTE				
	Acc	Sen	Spe	PPV	NPV	Acc	Sen	Spe	PPV	NPV
Intracardiac anomalies	95%	88.24%	97.67%	93.75%	95.46%	99.17%	97.06%	100%	100%	98.85%
Extracardiac vascular anomalies	100%	100%	100%	100%	100%	94.87%	70.46%	98.88%	91.18%	95.32%
Anomalies of aortic artery and its branches	100%	100%	100%	100%	100%	96.67%	85.71%	98.99%	94.74%	97.03%
Anomalies of the pulmonary vessels	100%	100%	100%	100%	100%	93.06%	50%	98.44%	80%	94.03%
Anomalies of the aortopulmonary vessels	100%	100%	100%	100%	100%	93.75%	75%	97.50%	85.71%	95.12%
Anomalies of the systemic veins	100%	100%	100	100%	100%	95.83%	50%	100%	100%	95.65%
Coronary artery anomalies	100%	100%	100%	100%	100%	91.67%	33.33%	100%	100%	91.30%
Total	98.61%	94.87%	99.44%	97.37%	98.88%	96.07%	82.05%	99.15%	95.52%	96.16%

Abbreviations: DSCT, dual-source computed tomography; TTE, transthoracic echocardiography; Acc, accuracy; Sen, sensitivity; Sep, specificity; PPV, positive predictive value; NPV, negative predictive value.

3.5. Assessment of image quality

DSCT scanning was performed successfully in all 24 patients, and the mean image quality score was 3.70 ± 0.47. 16(66.67%) patients got a score of 4,8(33.33%) patients gained 3. The interobserver agreement of overall image quality was calculated as κ = 0.81, which indicated excellent agreement.

3.6. Intra-observer and inter-observer variability

The ICCs of intra-observer variability were 0.91–0.98, and the ICCs of inter-observer variability were 0.87–0.97.

3.7. Radiation dose estimation

The estimated mean ED for patients aged younger than 4 months, between 4 months and 1 year old, between 1 and 6 years old, between 6 years and 10 years old,and older than 10 years were 1.25 ± 0.13 mSv, 0.98 ± 0.14mSv, 0.74 ± 0.31 mSv, and 0.70 ± 0.24 mSv, and 1.23 ± 0.34 mSv, respectively. The estimated mean ED was 0.98 ± 0.37mSv. (Table 5)

Table 5
Radiation dose estimation according to different age groups

	< 4 months	4 months to 1 year	1 year to 6 years	6 years to10 years	⩾10 years
CTDIvol(mGy)	4.14 ± 0.50	8.07 ± 3.52	8.04 ± 4.95	9.43 ± 0.71	9.87 ± 4.89
DLP(mGy·cm)	32.00 ± 3.27	39.00 ± 3.00	41.12 ± 17.16	58.67 ± 19.69	89.63 ± 24.39
ED (mSv)	1.25 ± 0.13	0.98 ± 0.14	0.74 ± 0.31	0.70 ± 0.24	1.23 ± 0.34

CTDIvol, volume CT dose index; DLP, dose-length product; ED, effective dose.

4. Discussion

PTA is an uncommon congenital cardiac abnormality that occurs due to conotruncal septation failure during fetal development and is correlated with chromosome 22q11 deletion and DiGeorge syndrome [20]. It is always accompanied by VSD and other cardiovascular abnormalities. An early surgical repair is an ideal option in its management. The accurate delineation of morphological characteristics

and associated cardiovascular anomalies are essential for the surgical strategies and outcomes. Thus, the exact preoperative diagnosis of these anomalies is imperative.

DSCT, with high temporal and spatial resolution, low radiation, and powerful post-processing techniques, could accurately visualize cardiovascular anomalies. Our study showed 13 patients of typeA1 and only one patient of type A4, which were the most and least common types, respectively. No type B patient was found. These results were entirely consistent with the results confirmed by surgery or CCA. The preoperative measurement of VSD on DSCT was valuable for VSD patch closure must be performed during the operation. The VSDs were always large, for the average diameter in our research was 1.46 ± 0.56cm. Also, the average diameter of TA,MPA□RPA and LPA can be measured on DSCT. These data could supply detailed quantitative information for the clinicians.

DSCT was superior to TTE in detecting associated cardiac vascular anomalies. It confirmed more accurately than TTE in all extracardiac groups in the present study. The main reasons could be the small field of view examined via suprasternal approach, the pneumatic lung, and the short neck of pediatric patients. Additionally, these structures in the neck and chest were shielded partly by the cervical and thoracic bones, which could also be responsible for the unsatisfactory diagnostic performance for TTE. Our data revealed that DSCT was inferior to TTE for the detection of intracardiac anomalies. The results could be partially attributed to the truth that DSCT is an imaging modality requiring a workstation to transfer digital information to gray-scale images [21].

Accurate preoperative diagnosis of coronary artery anomalies is critical. Firstly, during the surgical repair of PTA, the right ventricle's infundibulum needs to be incised before restoration of right ventricle-pulmonary artery continuity [22]. Therefore, any malformed coronary artery that goes across the right ventricle's infundibulum could be accidentally damaged during the right ventriculotomy. Secondly, coronary artery anomalies are significant risk factors for death after operation [23]. Our results showed that DSCT could detect this abnormality with 100% sensitivity and 100% specificity. Besides, in the PTA patients, the coronary arteries and pulmonary arteries originate from the truncus artery. It is crucial to identify the ostia number and location of coronary arteries because the coronary ostia or proximal coronary segments could be distorted during the excision of pulmonary arteries from the truncus artery. They could be showed and evaluated accurately by CT, While TTE could miss them [24].

The concomitant pulmonary artery abnormalities such as crossed pulmonary artery and pulmonary artery stenosis are essential in performing the surgery [6, 14]. In addition, during PTA surgical procedure, detachment of the pulmonary arteries from the arterial trunk was necessary to form a right ventricle to pulmonary artery conduit. So, a noninvasive assessment of the origins and route of pulmonary arteries was crucial. DSCT could provide detailed and comprehensive information about them through powerful post-processing techniques. With regards to aortopulmonary collateral arteries, accurate preoperative evaluation of these collateral arteries could be helpful in surgical planning [5, 25]. DSCT could easily identify the number, origin, branching pattern, and supplied lung lobes. However, only large collateral vessels could be demonstrated on TTE [26].

The radiation dose is a significant concern undergoing cardiac CT. In our series, several steps were made to reduce radiation dose. Firstly, tube voltage was one of the crucial factors affecting radiation exposure. The tube voltage was set at a low level of 80 kV in our study, which not only decreased the radiation exposure but also made higher cardiovascular enhancement without the loss of contrast-to-noise ratio [27]. Secondly, An ECG-gated sequential technique was used which reduced the radiation dose dramatically. Finally, the heart rhythm adaptive pitch was applied, which adapted higher pitch to fit higher heart rhythm. It reduced both radiation exposure and scanning time. In summary, the estimated mean ED was < 1mSv (0.98 ± 0.37mSv), which was under the ALARA (as low as reasonably achievable) principle.

Our study has several limitations. Firstly, because PTA is rare congenital heart disease, our single-center research had a relatively small number of patients. Further multi-center research is needed for larger sample enrollment. Secondly, radiation exposure is inevitable in CT scanning. Thus, we adopted several effective measures to minimize the radiation dose, and the estimated mean ED was 0.98 ± 0.34mSv, which was under the ALARA principle. Finally, as this is a retrospective study, the selection bias is inevitable.

5. Conclusions

In general, low-dose DSCT could accurately confirm the morphological features of PTA. Furthermore, it has advantages in diagnosing the associated cardiovascular malformations, compared with TTE. Nevertheless, some intracardiac anomalies could be missed by low-dose DSCT. Therefore, it would be beneficial to combine low-dose DSCT with TTE to provide more accurate information for clinical interventions.

Abbreviations

PTA: Persistent truncus arteriosus; TTE: Transthoracic echocardiography; DSCT: Dual-source computed tomography; CCA: Conventional cardiac angiography; TA: Truncus artery; MPA: Main pulmonary artery; RPA: Right pulmonary artery; LPA :Left pulmonary artery; VSD: Ventricular septal defect; CTDIvol: Volume CT dose index; DLP: Dose-length product; ED: The effective dose; ICC: Intraclass correlation coefficients

Declarations

Ethics approval and consent to participate

Approval was granted by Biomedical Research Ethics Committee of our hospital, Sichuan University (Chengdu, Sichuan, China; No.14-163), and informed consent was waived off.

Consent for publication

Not applicable

Availability of data and materials

The datasets used during the current study are available from the corresponding author on reasonable request.

Competing interests

The authors declare that they have no competing interests.

Funding

This work was financially supported by Sichuan Science and Technology Program (2020YJ0229) and 1·3·5 project for disciplines of excellence, West China Hospital, Sichuan University (ZYGD18013).

Authors' contributions

Conceived and designed the experiments: ST, QW. YL, ZY. Performed the experiments: ST, QW, KS, YG, LJ. Analyzed the data: ST, QW, LJ, JW, KS, ZG Y, YL. Contributed reagents/materials/analysis tools: ST, QW, KS, LJ, ZG Y, YL, JW. Wrote and review the paper: ST, QW. YL, ZY, YG. All authors read and approved the final manuscript.

Acknowledgements

Not applicable

References

1. Sharma A, Priya S, Jagia P. Persistent truncus arteriosus on dual source CT. Jpn J Radiol. 2016;34(7):486-93. https://doi:10.1007/s11604-016-0559-x
2. Martin BJ, Ross DB, Alton GY, Joffe AR, Robertson CM, Rebeyka IM, et al. Clinical and Functional Developmental Outcomes in Neonates Undergoing Truncus Arteriosus Repair: A Cohort Study. Ann Thorac Surg. 2016;101(5):1827-33. https://doi:10.1016/j.athoracsur.2015. 10.114
3. Kharwar RB, Dwivedi SK, Chandra S, Saran RK. Persistent truncus arteriosus: a rare survival beyond the first decade. J Am Coll Cardiol. 2014;63(17):1807. https://doi:1016/j.jacc.2013.12.054
4. Naimo PS, Fricke TA, Yong MS, d'Udekem Y, Kelly A, Radford DJ, et al. Outcomes of Truncus Arteriosus Repair in Children: 35 Years of Experience From a Single Institution. Semin Thorac Cardiovasc Surg. 2016;28(2):500-511. https://doi:10.1053/j.semtcvs.2015.08.009

5. Fujiwara K, Yoshizawa K, Kato O, Sakazaki H. Truncus Arteriosus With Major Aortopulmonary Collateral Arteries. Ann Thorac Surg. 2019;108(2):e105-e106. https://doi:10.1016/j.athoracsur.2018.12.051

6. Morgan CT, Tang A, Fan CP, Golding F, Manlhiot C, van Arsdell G, et al. Contemporary Outcomes and Factors Associated With Mortality After a Fetal or Postnatal Diagnosis of Common Arterial Trunk. Can J Cardiol. 2019;35(4):446-452. https://doi:1016/j.cjca. 2018. 12.006

7. Shi K, Yang ZG, Xu HY, Zhao SX, Liu X, Guo YK. Dual-source computed tomography for evaluating pulmonary artery in pediatric patients with cyanotic congenital heart disease: Comparison with transthoracic echocardiography. Eur J Radiol. 2016;85(1):187-192. https://doi:10.1016/j.ejrad.2015.11.002.

8. Zhang Y, Yang ZG, Yang MX, Shi K, Li R, Diao KY, et al. Common atrium and the associated malformations: Evaluation by low-dose dual-source computed tomography. Medicine (Baltimore). 2018;97(46): e12983. https://doi:10.1097/MD.0000000000012983.

9. Nie P, Wang X, Cheng Z, Ji X, Duan Y, Chen J. Accuracy, image quality and radiation dose comparison of high-pitch spiral and sequential acquisition on 128-slice dual-source CT angiography in children with congenital heart disease. Eur Radiol. 2012;22(10):2057-66. https://doi:10.1007/s00330-012-2479-1.

10. Shi K, Gao HL, Yang ZG, Zhang Q, Liu X, Guo YK. Preoperative evaluation of coronary artery fistula using dual-source computed tomography. Int J Cardiol. 2017; 228:80-85. https://doi:10.1016/j.ijcard.2016.11.169

11. Jiang L, Xie LJ, Yang ZG, Shi K, Xu HY, Li R, et al. Preoperative evaluation of anomalous pulmonary venous connection using dual-source computed tomography: Comparison with echocardiography. Eur J Radiol. 2017; 94:107-114. https://doi:10.1016/j.ejrad.2017.06.015

12. Yang MX, Yang ZG, Zhang Y, Shi K, Xu HY, Diao KY, et al. Dual-source Computed Tomography for Evaluating Pulmonary Artery and Aorta in Pediatric Patients with Single Ventricle. Sci Rep. 2017;7(1):13398. https://doi:10.1038/s41598-017-11809-6

13. Groves DW, Olivieri LJ, Shanbhag SM, Bronson KC, Yu JH, Nelson EA, et al. Feasibility of low radiation dose retrospectively-gated cardiac CT for functional analysis in adult congenital heart disease. Int J Cardiol. 2017; 228:180-183. https://doi:10.1016/j.ijcard.2016.11.108.

14. Talwar S, Rajashekar P, Gupta SK, Gulati GS, Airan B. Crossed Pulmonary Arteries in a Patient With Persistent Truncus Arteriosus. Ann Thorac Surg. 2016;101(6):2377-9. https://doi:10.1016/j.athoracsur.2015.07.069

15. Turkoglu S, Batur A, Yokuş A, Dündar İ, Akinci MB. Contrast enhanced computed tomography findings of persistent truncus arteriosus; A rare congenital heart disease. Radiol Case Rep. 2020;15(6):795-798. https://doi:1016/j.radcr.2020.04.007

16. Furuta A, Nagashima M, Hiramatsu T, Matsumura G, Yamazaki K. Surgical repair of a truncus arteriosus with unilateral absence of the right proximal pulmonary artery. J Card Surg. 2016;31(11):703-705. https://doi:10.1111/jocs.12848

17. Van Praagh R, Van Praagh S. The anatomy of common aorticopulmonary trunk (truncus arteriosus communis) and its embryologic implications. A study of 57 necropsy cases. Am J Cardiol. 1965;16(3):406-25. https://doi:10.1016/0002-9149(65)90732-0

18. Brady SL, Mirro AE, Moore BM, Kaufman RA. How to Appropriately Calculate Effective Dose for CT Using Either Size-Specific Dose Estimates or Dose-Length Product. AJR Am J Roentgenol. 2015;204(5):953-8. https://doi:10.2214/AJR.14.13317

19. Narayan HK, Finkelman B, French B, Plappert T, Hyman D, Smith AM, et al. Detailed Echocardiographic Phenotyping in Breast Cancer Patients: Associations With Ejection Fraction Decline, Recovery, and Heart Failure Symptoms Over 3 Years of Follow-Up. Circulation. 2017;135(15):1397-1412. https://doi:10.1161/CIRCULATIONAHA.116.023463

20. McElhinney DB, Driscoll DA, Emanuel BS, Goldmuntz E. Chromosome 22q11 deletion in patients with truncus arteriosus. Pediatr Cardiol. 2003;24(6):569-73. https://doi:10.1007/s00246-003-0441-3

21. Shi K, Yang ZG, Chen J, Zhang G, Xu HY, Guo YK. Assessment of Double Outlet Right Ventricle Associated with Multiple Malformations in Pediatric Patients Using Retrospective ECG-Gated Dual-Source Computed Tomography. PLoS One. 2015;10(6): e0130987. https://doi:10.1371/journal.pone.0130987

22. Alamri RM, Dohain AM, Arafat AA, Elmahrouk AF, Ghunaim AH, Elassal AA, et al. Surgical repair for persistent truncus arteriosus in neonates and older children. J Cardiothorac Surg. 2020;15(1):83. https://doi:10.1186/s13019-020-01114-1

23. Bonilla-Ramirez C, Ibarra C, Binsalamah ZM, Adachi I, Heinle JS, McKenzie ED, et al. Coronary Artery Anomalies Are Associated with Increased Mortality After Truncus Arteriosus Repair. Ann Thorac Surg. 2020: S0003-4975(20)31908-1. https://doi:10.1016/j.athoracsur.2020.08.082

24. Cook SC, Raman SV. Unique application of multislice computed tomography in adults with congenital heart disease. Int J Cardiol. 2007;119(1):101-6. https://doi:10.1016/j.ijcard.2006.07.074

25. Dillman JR, Hernandez RJ. Role of CT in the evaluation of congenital cardiovascular disease in children. AJR Am J Roentgenol. 2009;192(5):1219-31. https://doi:2214/AJR.09.2382

26. Chandrashekhar G, Sodhi KS, Saxena AK, Rohit MK, Khandelwal N. Correlation of 64 row MDCT, echocardiography and cardiac catheterization angiography in assessment of pulmonary arterial anatomy in children with cyanotic congenital heart disease. Eur J Radiol. 2012;81(12):4211-7. https://doi:10.1016/j.ejrad.2012.08.010

27. Faggioni L, Neri E, Sbragia P, Pascale R, D'Errico L, Caramella D, et al. 80-kV pulmonary CT angiography with 40 mL of iodinated contrast material in lean patients: comparison of vascular enhancement with iodixanol (320 mg I/mL) and iomeprol (400 mg I/mL). AJR Am J Roentgenol. 2012;199(6):1220-5. https://doi:10.2214/AJR.11.812

Figures

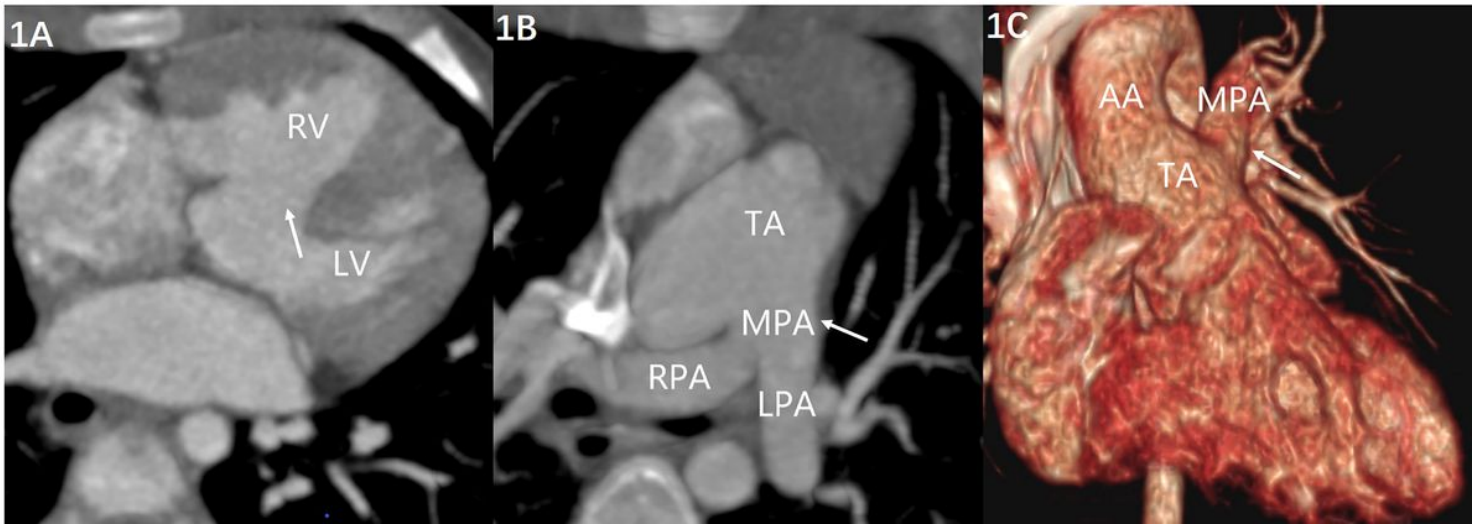

Figure 1

Type A1 persistent truncus arteriosus in a two years old male. (A) Axial maximum intensity projection (MIP) image displays the ventricular septal defect (arrow). (B) The axial MIP image and (C) The volume rendering (VR) image demonstrates that a single MPA arises from the proximal left lateral aspect of the TA (arrow), then brunches into RPA and LPA. RV, right ventricle; LV, left ventricle; TA, truncus artery; MPA, main pulmonary artery; RPA, right pulmonary artery; LPA, left pulmonary artery; AA, ascending aorta

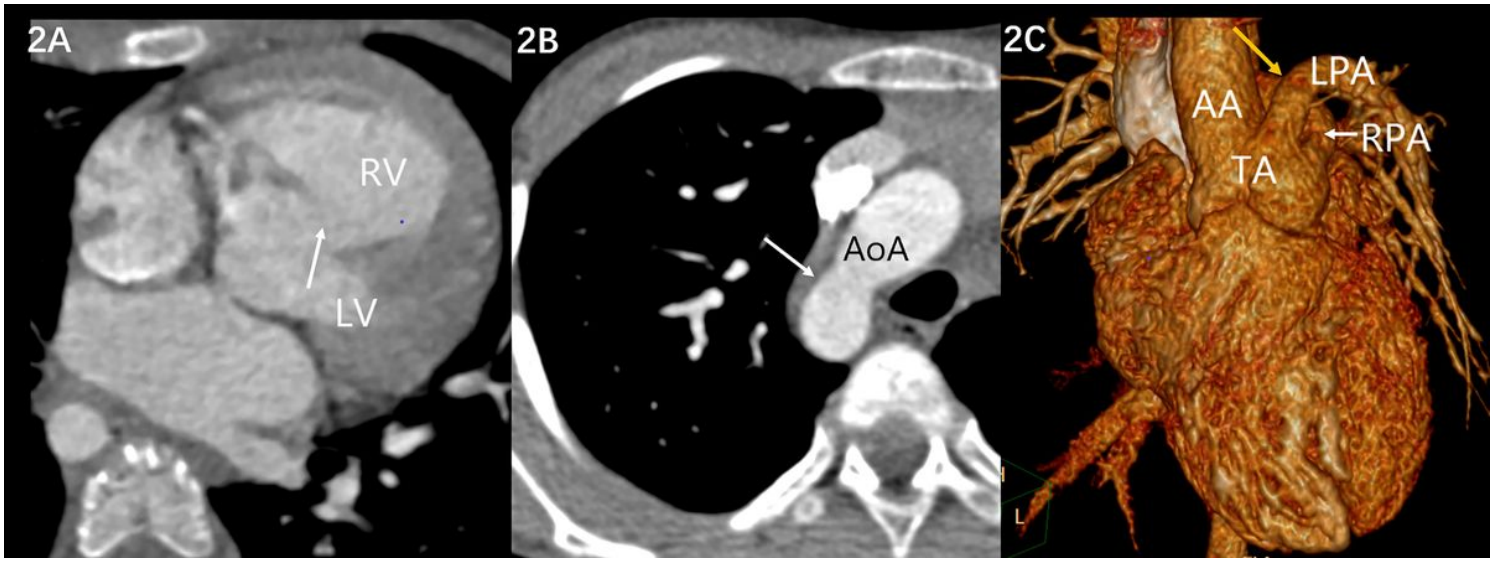

Figure 2

Type A2 persistent truncus arteriosus in a ten years old female. (A) Axial image shows the ventricular septal defect (arrow). (B) Axial image displays the right-sided AoA. (C) The volume rendering (VR) image demonstrates that a close but separate origin of RPA and LPA from the proximal left lateral aspect of the TA, then cross to the opposite lung, which was called crossed pulmonary artery (yellow arrow). RV, right ventricle; LV, left ventricle; AoA aortic arch; TA, truncus artery; RPA, right pulmonary artery; LPA, left pulmonary artery; AA, ascending aorta

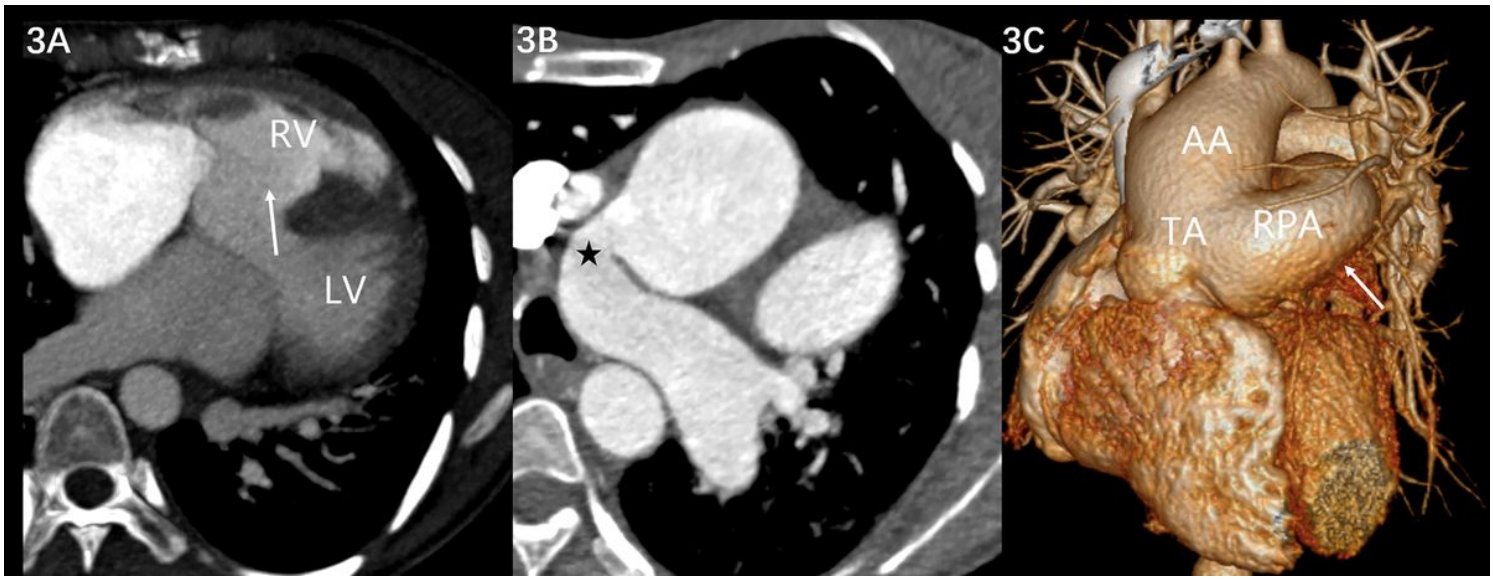

Figure 3

Type A3 persistent truncus arteriosus in 26 years old female. (A) Axial maximum intensity projection (MIP) image displays the ventricular septal defect (arrow). (B) Axial image depicts a large vessel arises from the aortic arch to supply the left lung (black star). (C) The volume rendering (VR) image demonstrates the RPA originating from the proximal left lateral aspect of the TA (arrow). RV, right ventricle; LV, left ventricle; TA, truncus artery; RPA, right pulmonary artery; AA, ascending aort

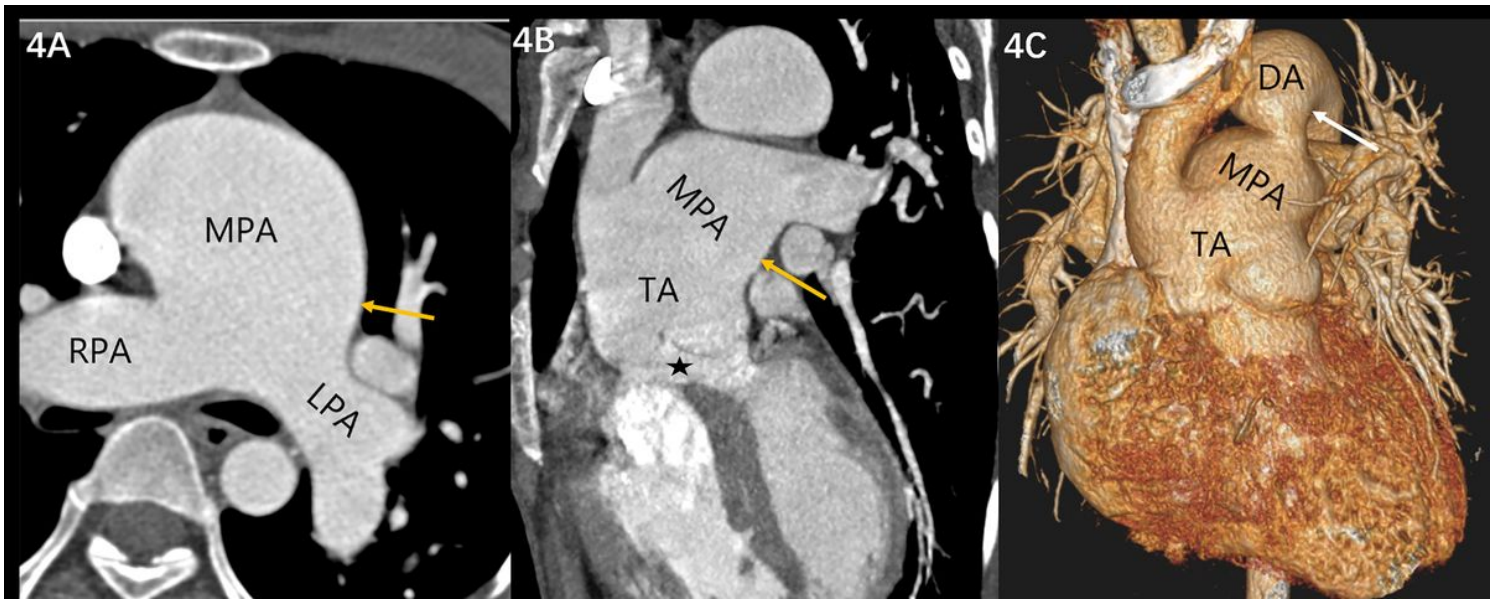

Figure 4

Type A4 persistent truncus arteriosus in 27 years old female. (A) The axial image demonstrates a single MPA arising from the TA (arrow). (B) Multiple planar reconstruction (MPR) image shows the presence of MPA (arrow) and ventricular septal defect (black star). (C) The volume rendering (VR) presents interrupted aortic arch with DA arising from MPA directly (arrow). MPA, main pulmonary artery; RPA, right pulmonary artery; LPA, left pulmonary artery; TA, truncus artery; DA, descending aorta

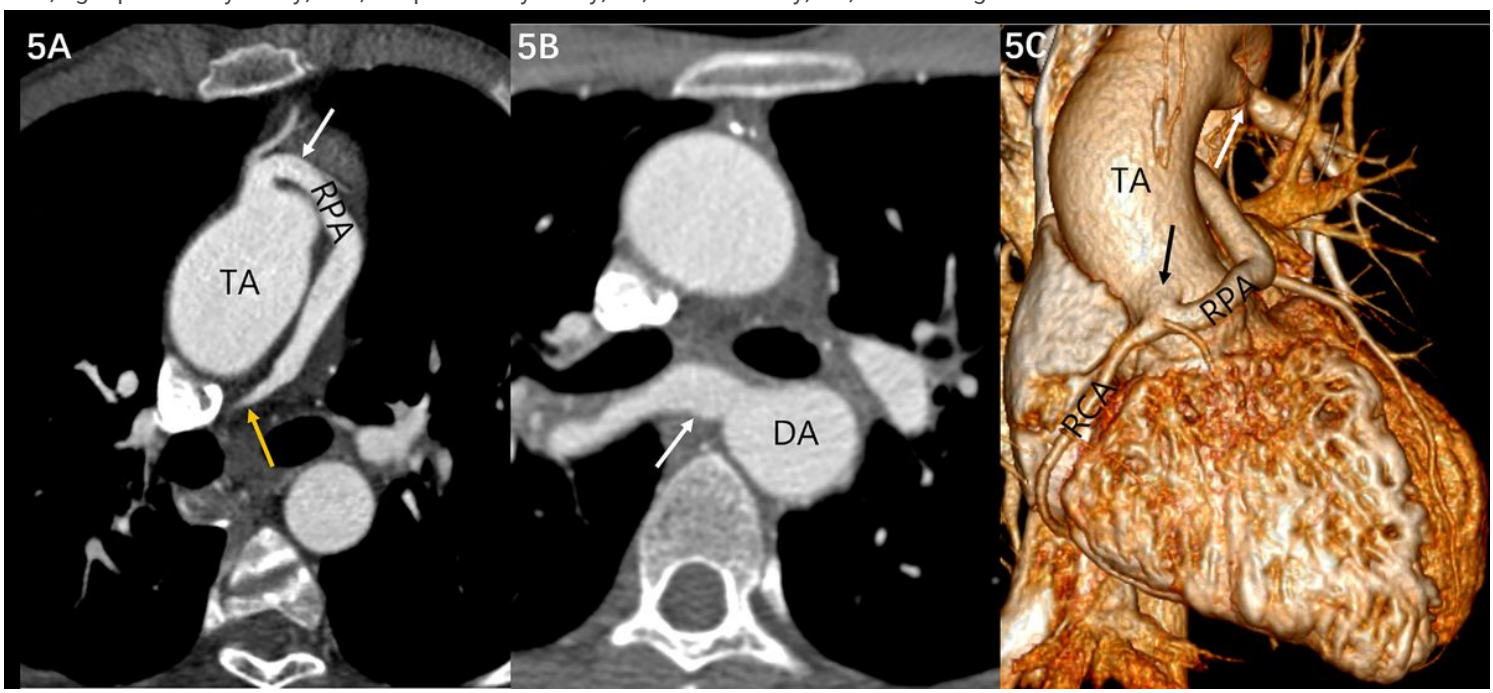

Figure 5

Persistent truncus arteriosus in 21 years old male with abnormalities of coronary and pulmonary arteries. (A) Axial image shows the RPA arising from the TA (white arrow) and the pulmonary artery stenosis (yellow arrow). (B) Axial image demonstrates a large aortopulmonary collateral vessel from the DA (arrow). (C) The volume rendering (VR) shows that RPA and RCA originate from the same site of TA (black arrow) and pulmonary artery stenosis of LPA (white arrow). TA, truncus artery; RPA, right pulmonary artery; DA, descending aorta; RCA, right coronary artery. LPA, left pulmonary artery.